

IIII ISPS-6 Proceedings IIIII
(Review)

X-RISE - A Multifunctional X-ray Radiography Device for Parabolic Flights and Laboratory Use

Stefan KLEIN¹, Dirk BRÄUER¹, Maike BECKER¹, Alexander KNIPSTEIN^{1,2}, Sebastian MECKEL^{1,3},
Elke SONDERMANN¹ and Florian KARGL¹

Abstract

A multifunctional X-ray radiography device for parabolic flights and lab-based research is presented. Based on the technology demonstrator X-ray radiography facility DIXI for the Materials Science Laboratory aboard the International Space Station, the full 90° tiltability of the facility enables to change the gravity vector with respect to the sample orientation, providing the tunability of the impact of the gravitational force on the investigated processes. The acronym X-RISE - X-Ray Investigations in Space Environment - unifies our research activities by utilizing a X-ray micro-radiography facility for different experiment classes with the need for microgravity environment namely solidification research, diffusion experiments, and the dynamics of granular matter upon compaction. A commercial actively pumped microfocus transmission X-ray source by Viscom AG delivers up to 20W X-ray power at 100 kV acceleration voltage. It is combined with different experiment cartridges and detector modules. The facility is classified as a fully-protected radiography equipment according to German and French radiation safety laws. Besides its use aboard parabolic flights it is also a powerful terrestrial research facility. The technological possibilities of X-RISE for material science research are presented within this paper. Moreover examples of recent parabolic flight experiments focusing on different science areas are presented to highlight the capabilities of this facility.

Keyword(s): In-situ X-ray radiography, Solidification, Diffusion, Metallic alloys, Granular matter

Received 20 October 2015; Accepted 18 July 2016; Published 31 October 2016

1. Introduction

X-ray synchrotron radiation radiography and tomography techniques have been increasingly used in the past 10 years to study processes in-situ, covering a broad range of research areas from biology¹⁾, to medicine²⁾, and to materials science^{3,4)}. The step from in-situ radiography to in-situ tomography was facilitated by advanced X-ray sources as well as improved detectors and sample processing techniques.

In materials sciences X-ray radiography was used to study materials processes like diffusion⁵⁾ and solidification in real-time and in-situ⁶⁻⁸⁾ with increasing precision. This enables to understand the fundamental processes but also to revise previously obtained results with larger errors. Fast high resolution area detectors and highly brilliant synchrotron sources enabled to study phenomena like dendritic solidification of metals^{3,6,9,10)}. However, from the synchrotron experiments it became apparent that convective fluid flow largely affects the experiments^{11,12)} and some of the experiments show the need for a microgravity environment to avoid gravity caused effects as for example buoyancy-driven convective fluid flow in liquid metallic alloys¹³⁾.

The development of compact transmission microfocus X-ray sources enables the scientists to perform some of the in-situ X-ray

radiography experiments in their own laboratories¹⁴⁾. We present a multifunctional X-ray radiography device (X-RISE) which can be vertically rotated by 90° in order to change the influence of the gravity on the samples with respect to the direction of the X-ray beam. Moreover it can be operated on microgravity platforms like parabolic flights.

The versatility of the X-RISE device allows to develop new research fields beyond dendritic solidification of metallic alloys like unconsolidated granular media. In the following we present the technical details of the facility and provide examples of recent parabolic flight experiments covering diffusion of Al-Cu alloys, solidification of an Al-Ge alloy and granular compaction of a loose non-agitated granular assembly.

2. Experimental Setup

Figure 1 shows a photograph of the X-RISE facility installed aboard the A300 ZERO-G operated by the french company NOVESPACE during the 24th DLR parabolic flight campaign. NOVESPACE is contracted by the French, German, and European space agencies CNES, DLR, and ESA to carry out several parabolic flight campaigns per year with differing agency

1 Institut für Materialphysik im Weltraum, Deutsches Zentrum für Luft- und Raumfahrt, 51170 Köln, Germany

2 Rheinische Fachhochschule Köln - University of Applied Sciences 50825 Köln, Germany.

3 Zentrum für Marine Umweltwissenschaften der Universität Bremen, 28359 Bremen, Germany
(E-mail: stefan.klein@dlr.de)



Fig. 1 Photograph of the X-RISE facility aboard the A300 Zero-G of NOVESPACE. The rack on the left hand side hosts the experiment control equipment, whereas in the rack on the right hand side, the X-ray experiment unit is located.

involvement. Despite the safety requirements, the challenge during building the X-RISE facility was to keep it as compact and light in weight as possible and with respect to the different experiments as versatile and modular as possible. To this end the X-RISE facility consists of two major parts, the control rack (left) and the experiment rack (right), and modular elements as spacer rings for adapting the magnification of the X-ray images, different experiment cartridges including an universal cartridge with standardized connections, and experiment specific control boxes in the form of slide-in modules which make X-RISE a powerful multifunctional X-ray device. The logical conjunction of the two racks and of the main parts are shown in the appendix.

2.1 Control Rack (Figure 1, Left)

The control rack (cf. **Fig. 1**, left) is equipped with two computer consoles: one for X-ray control including image recording and detector operation and one to control the experiment installed in the sample environment chamber. For control of the X-ray source the LabEx software (Fraunhofer IIS/EZRT, Erlangen) is utilized¹⁵⁾. A related control box (cf. top **Fig. 2**) hosts the control boards and the 24 V and 40 V power supply to run the X-ray generator which is part of the X-ray unit inside the experiment rack.

Customized LabView programs are used to control for example controlling and monitoring the temperature of furnace inserts. The temperatures are controlled by a dual zone PID-controller featuring a feedforward control and static decoupling of the thermal zones. Temperature time profiles can be pre-defined which is important for parabolic flight campaigns where the time-line for the parabolas are well defined and live operations are difficult. The experiment specific wiring and if needed additional controllers for engines are mounted inside the experiment specific control box and its slide-in module, respectively (cf. **Fig. 2**, bottom).

Apart from control soft- and hardware, the control racks are equipped with additional drawers to store up to two additional experiment cartridges and one additional experiment specific slide-in module which can be used for in-flight experiment changeovers. Moreover two EA-PS 8080 power supplies which deliver up to 1500 W each are part of the control rack. At the same time, either output voltages can be generated up to 80 V or output currents up to 40 A.

2.1.1 Experiment Specific Control Box

The experiment specific slide-in module of the control box offers a volume of about $(300 \times 195 \times 136) \text{ mm}^3$ and is equipped with a standardized set of electrical D-sub connectors at the backplate. Two high power D-sub connectors offer access to 230 VAC and 24 VDC, respectively, to power the additional equipment in the slide-in module. Four additional standard connectors are linked to a National Instruments (NI) Compact DAQ System and via USB to the LabView computer. Beside an USB Connection for multipurpose use, two NI thermocouple input modules (NI 9211) with a total of 8 channels, a module with 32 digital

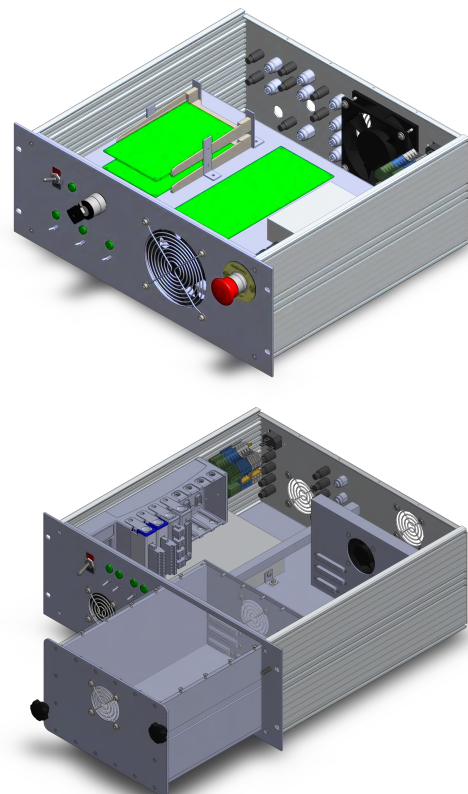


Fig. 2 Control-boxes for the X-ray and detector modules equipped with the X-ray control boards (green) and power supplies (light gray) and for the experiment with its NI-Compact DAQ System (left side with blue colored inserts), power supplies, and the experiment specific control box (sliding part) at the bottom.

input/output channels (NI 9205), and a module with 4 universal analog input channels (NI 9403) are available as a standard to the different experiments. Which of the channels and connections are used depends on the individual experiments. Four further slots for NI modules are available. Beside the experiment specific equipment a pressure sensor and two reference thermocouples are connected to the DAQ System. The pressure sensor is used to monitor the sample area pressure if required. The two thermocouples can be used to measure equipment temperatures at various freely selectable positions. For instance for high temperature furnace operation and in-flight changeover, the cartridge front-plate temperature has to be monitored.

2.2 Experiment Rack

The experiment rack (cf. **Figs. 3** and **4**) hosts the X-ray experiment unit. This unit consists of an actively pumped X-ray source (contained in the blue part) providing the cone-shaped X-ray beam. The vacuum for the source is build up by a turbomolecular pump (Pfeiffer HiPace10) in combination with a 24 V powered diaphragm pump (Pfeiffer MVP20). On top of the X-ray source the sample chamber (red) is mounted. The chamber has a shelf to integrate the experiment cartridge (purple). An additional spacer-ring (orange) could be used to change the magnification of the radiographs. Either by adding the ring between the X-ray source and the sample chamber or by adding the ring between the sample chamber and detector module (green) as shown in **Fig. 3** completing the X-ray experiment unit. Furthermore, the experiment rack contains a closed cooling water loop propelled by a Flojet Quad Pump (powered by 24 V, flow rate 12.5 l/min, and up to 2.4 bar). The cooling loop is used for the X-ray source by cooling the front-plate to which the X-ray source is mounted, the detector module, and finally, if required, the sample cartridge in the above mentioned sequence. The cooling water is streamed through heat exchanger plates coupled to the rack structure. An additional pumping unit to evacuate the experiment cartridge (or directly the sample chamber), if needed, is available inside the rack. The pumping unit consists of a turbomolecular pump (Leybold TW70) and a second diaphragm pre-pump (Pfeiffer MVP20). For in-flight operation the entire rack is water-tight closed by means of transparent Makrolon shielding, to prevent the cooling water from being ejected into the airplane in case of a cooling loop failure.

One of the unique characteristic of X-RISE despite the utilization aboard the A300 Zero-G aircraft is that the superstructure of the experiment facility as X-ray unit, sample chamber including the experiment cartridge, and detector module are mounted onto a rail (cf. yellow part in **Fig. 3**) which is rotatable mounted in the rack (cf. **Fig. 4**). As a consequence the experiment facility can be tilted 90° between horizontal and vertical alignment (cf. **Fig. 4**). This alignment enables the X-ray radiation to change between a horizontal beam direction and a vertical beam direction

with respect to the gravitational force. In case of ground based in-situ X-ray radiography experiments of dendritic solidification of quasi 2-dimensional metallic alloys, buoyancy-driven fluid flow can be suppressed by aligning the thin sample perpendicular to the gravitational force¹⁶).

For a better visualization the different parts of the X-ray unit are displayed in **Fig. 3** unclosed and colored in an exploded view. The compact, light weighting microfocus X-ray tube (Viscom) with its compact turbomolecular pump and high voltage generator has its best resolution with the smallest beam-size of about 3 μm. That can be realized at low power operation of the source (< 4 W). Further information on the microfocus X-ray source are given elsewhere¹⁷).

The radiographs are recorded by one out of the three available detector modules. One detector has a 49.2 × 49.3 mm² RadEye2 sensor with a Scint-X scintillator at 48 μm per pixel resolution with a 14 bit dynamic range. The record speed could be up to two frames per second. The same sensor with a structured CsI scintillator itemizes the second detector. The third detector is a CCD-/COOL-1100XR with a 100 μm structured CsI scintillator

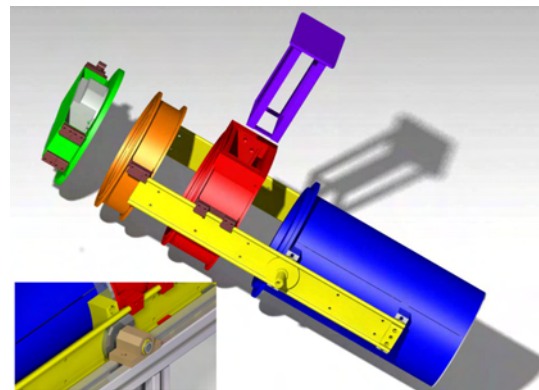


Fig. 3 Exploded diagram of the X-RISE facility; microfocus X-ray unit (blue), sample environment chamber (red), experiment cartridge (purple), optional chamber extension (orange), detector module (green). The picture detail in the lower left show the rotatable suspensions of the X-ray device.

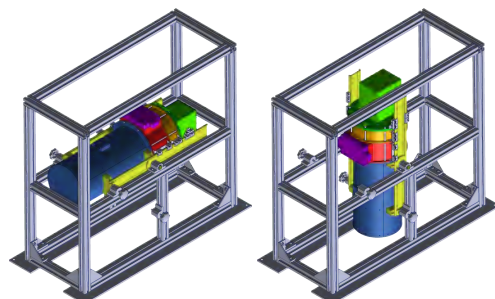


Fig. 4 The experiment rack with the rotatable X-ray experiment unit shown in horizontal (left) and vertical (right) position with respect to the gravitational force. Size of the experiment rack is about 440mm × 1090mm × 1000mm

and a pixel size of $9 \times 9 \mu\text{m}^2$. Recording with a resolution of 4016×2680 pixels and 12-bit depth at up to 3 fps could be realized. By binning 2×2 pixels the recording speed could be increased to 6 fps.

2.2.1 Experiment Cartridges

The latest and most universal version of the experiment cartridge has a unified set of feed-troughs for vacuum, cooling water, and electricity (cf. **Fig. 5**). In case of operating resistance heating furnaces, a medium vacuum environment is needed to protect the heater materials from burning and the samples from a strong oxidization. The cartridge housing could be water cooled if needed. Therefore Cu-tubes are pressed in channels of the cartridge body made out of Aluminum and fixed with metal adhesive. Additional cooling water feed-troughs are available to actively cool parts inside the cartridge as for example a motor or a heat sink. In total 36 electrical connections are available. Two high current LEMO connectors (red circled connectors in **Fig. 5** bottom) with two electrical pins sustaining 40 A each can be used for resistance heating. The resistance heaters of the existing furnaces are powered by two EA-PS 8080 power supplies described above. Two additional LEMO connectors with 10 (purple circled connector) and 12 (green circled connector) electrical pins respectively can be used for thermocouples and engine control or any other needed wiring. The available volume for the experiments depends if either a cartridge is used or the sample chamber itself hosts the experiment. The largest vacuum cartridge provides a volume of $(135 \times 89 \times 280) \text{ mm}^3$. In order to minimize the X-ray adsorption by the 2 mm thick bottom and top Aluminum plate of the vacuum experiment cartridge, the areas where the X-ray beam transmits the cartridge are milled down to 0.5 mm. The maximum acceptable cartridge temperatures are 80°C at the front plate where the LEMO-connectors define the temperature limit and 110°C at the back. The limit of the back is set by the used rubber gaskets. In case a larger volume is needed to install an experiment the sample chamber itself could be used. By doing so a cylindrical volume of about 5.4 liters ($r = 132.5 \text{ mm}$, height $h = 98 \text{ mm}$) becomes available. The experiment could be mounted either on the front plate of the X-ray tube or on an open structure attached to the cartridge front plate hosting the needed feed-troughs. The front plate of the cartridge is covered by lead in order to keep scattered X-ray emission through the front-plate below the maximum allowed X-ray radiation limits for a fully-protected X-ray equipment.

As mentioned above several different experiment cartridges are already developed.

1. Beside the cartridge designed to monitor granular compaction by measuring the integrated fluctuations of particle positions¹⁸⁾, the other cartridges are conceptualized to investigate dynamic processes of liquid metals.
2. A second cartridge houses an isothermal furnace¹⁶⁾ which is used to investigate the equiaxed microstructure evolution

and grain interaction upon metal alloy solidification. Therefore, a temperature gradient $< 0.5 \text{ K/mm}$ across the quasi 2D sample is required which could be realized by our isothermal furnace (ITF) concept (cf. **Fig. 5**)¹⁶⁾.

3. Despite the physics behind equiaxed microstructure evolution, the transition from columnar to equiaxed grain growth (CET)^{9,19)} is an interesting solidification phenomenon which is relevant to casting industry. X-ray radiography in combination with temperature gradient furnaces (GF) is a suitable method to study the CET. A recently developed

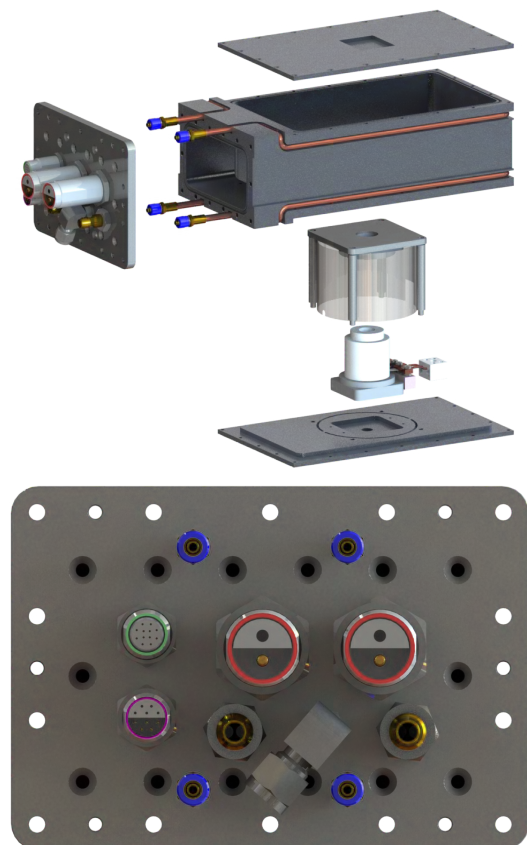


Fig. 5 Explosion diagram of the experiment cartridge (cf. **Fig. 3** purple part) hosting the ITF (top). X-rays penetrate the cartridge from the bottom to the top. The cartridge is equipped with an outerwall cooling system consisting of copper pipes which are pressed and glued into the Al-body. Bottom: The water connections of the front plate are shown in blue. The universal set of self-locking LEMO feed-throughs including the two high current connectors sustaining 40 A each could be used for resistance heating (red). A 10 pin (purple) and 12 pin (green) connector could be used for driving motors and reading temperatures for instance. Moreover two additional openings could be used for additional water cooling inside the cartridge (gold). The cartridge is designed to be evacuated through an additional port inside the front plate (Swagelok interface, gray 90° angled part).

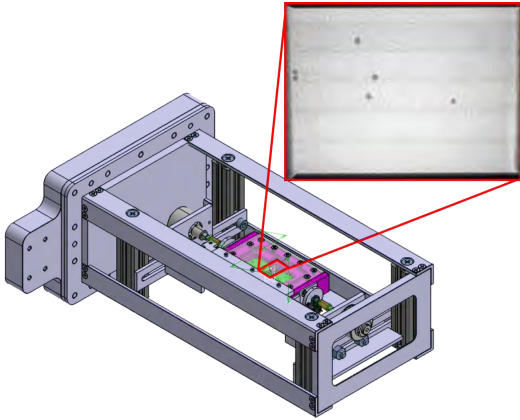


Fig. 6 Scheme of the GFC-cartridge filled with 8000 glass particles and a corresponding radiograph (top-right). X-rays penetrate the cartridge from the bottom to the top.

gradient furnace insert for X-RISE is currently under testing and first results will be published soon. The furnace is tested up to 870 K with a maximum temperature gradient of about 13 K/mm.

4. As a last example a very compact and linearly operated shear-cell (LSC)^{5,20} is integrated in an experiment cartridge to investigate the impact of gravity on diffusion in a periodically changing gravitational field during parabolic flights under different orientations of this field with respect to the capillary axis. A ultra-high temperature version of the shear-cell furnace is currently under development and will allow to process samples at temperature up to 1800°C.

Figure 5 shows an exploded view of the most universal cartridge hosting the isothermal furnace (ITF) for near equilibrium solidification studies of equiaxed dendrites. The copper tubes for cooling the cartridge walls by water are diagrammed and the fittings are colored in the drawing of the front plate. The vacuum feed-through is realized by a Swagelok interface. The electrical LEMO connectors are highlighted in green, purple, and red. The set of connectors can be used for different purposes and allow to perform the following different experiments where resistant heating via the two high current connectors (red) is realized. In case furnaces are operated the 12 pin connector (green) is applied for up to five thermocouples and a PT100 as precision resistor. The thermocouples are used to read and consequently to control the temperatures of the experiments. If additional connections as for instance to control an actuator are needed, the 10 pin feed through (purple) could be used.

2.2.2 The Granular Flow Cartridge - GFC

The sample cell of the granular experiment and a corresponding radiograph is shown in **Fig. 6**. The main part of the cell containing 8,000 glass beads of diameter 500 μm is a rectangular

frame (Teflon) in which two pistons (Teflon) could be moved in order to create a variable volume. Between the two pistons the granular matter is stored. The front and the back of the frame is closed with plates made of Makrolon. The frame has 4 holes on the side (two on the left side, two on the right side). Two holes will be used for position limit switches, to stop the linear motion of the pistons before hitting the side walls. The other two holes are for the piston rods (piston rods are made of steel). In these holes rod seals are mounted to prevent that granular particles escape the probe cell. The whole cell is mounted with screws and fixing brackets on a base plate (made of aluminum) which is implemented in the frame of the cartridge. By a parabolic flight campaign with X-RISE it has been shown that X-ray radiography allows for the observation of the compaction of a granular packing in microgravity. The conditions on parabolic flights are especially suitable to observe rattlers that are agitated by the rest-accelerations without destroying the packings.

For the measured data it is possible to quantify the bulk dynamics in the samples, resulting in much more reliable statistics. Using the time gradient by analyzing the difference images from the detector, a reliable quantity $\Delta(t)$ can be obtained to characterize the motion of the particles. $\Delta(t)$ allows the distinction between agitated and arrested states. In addition, it is possible to identify a novel regime of cooling quantitatively for low rates of compaction. This is only possible in microgravity as under the dominating influence of gravity granular gases collapse quite rapidly²¹). The newly identified cooling extends over several seconds and is described reasonably well by a linear decay of $\Delta(t)$ ¹⁸).

2.2.3 Isothermal Furnace - ITF

In a recently published paper the authors have developed an axis-symmetric furnace which achieves near-isothermal conditions within the Field of View (FoV) of a thin metallic sample to observe its solidification. Fortunately X-RISE can be rotated with respect to the gravity vector to enable in-situ studies of the



Fig. 7 Radiographs recorded with the X-RISE facility under terrestrial conditions during the solidification of an Al-Ge alloy. The image on the left was taken under vertical configuration (quasi 2D sample perpendicular to the gravitational force). The image on the right was taken in horizontal alignment of X-RISE. Here the gravity vector point from top to the bottom of the image. The diameter of the circular samples is 12 mm.

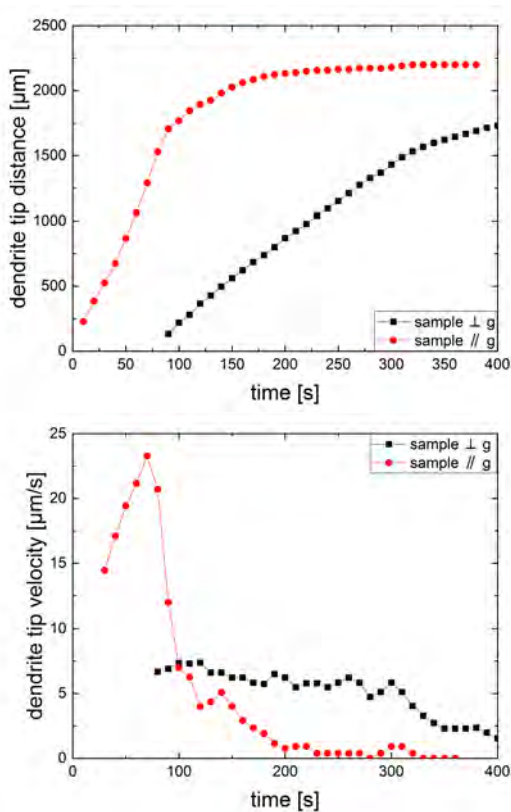


Fig. 8 The graphs show either the distance versus time (top) or growth velocities versus time (bottom) of two solidification experiments of the same Al-Ge sample. The tip distances are extracted from the individual radiography images by measuring the number of pixels from the dendrite center to a particular dendrite tip and converted into the proper length scales [μm]. The correlation with time results in the corresponding growth velocities. The black curves were extracted from an experiment with vertical alignment of X-RISE (suppressed fluid-flow) and the data displayed in red were taken while X-RISE was horizontally aligned (buoyancy flow). In both cases the cooling rate was 1 K/s.

effects of gravity on alloy solidification in the laboratory. For further information the reader is kindly referred to the publication of Becker et al.¹⁶⁾

Figure 7 shows two different radiography images of an intermediate stage of the solidification event of an Al-Ge alloy. The image on the left was taken during an experiment which was performed in vertical alignment of the X-ray experiment unit. In this particular case the gravity driven fluid flow was shown to be suppressed¹⁶⁾. The image on the right was taken with a vertically 90° tilted X-ray unit resulting in a horizontal X-ray beam and the thin sample aligned parallel to the gravitational force. Buoyancy-driven fluid flow leading to a flow of the denser liquid in the direction of the gravitational force becomes visible within the live video. However, the fluid flow also changes the morphology of the equiaxed growing dendrite in such a way that the branch of the dendrite growing opposite to the fluid flow stream grows much

faster than the branch of the dendrite growing parallel with the fluid flow^{22–24)}. This can be also seen in the two images shown in **Fig. 7**. Whereas for the horizontal sample the dendrites appear rather symmetric with typically 6 nicely developed branches, for the vertical sample alignment the dendrites are highly non-symmetric with typically 1 to three longer branches and a short branch opposing the long one.

2.2.4 Solidification Experiments

Figure 8 shows data of two different experiments carried out under terrestrial conditions. Black curves were determined from a sample oriented perpendicular with respect to the gravitational force and red data points were extracted from a quasi 2D-sample solidified in parallel to the gravity vector. The graph above shows the dendrite evolution as distance versus time whereas the bottom graph shows the dendrite tip velocities versus time. The data were extracted from the marked dendrites in **Fig. 7**. For horizontal alignment of the source, obviously the dendrite which grows antiparallel to the gravitational force is much longer than the other branches of the grain. In order to extract the growth velocities versus time every tenth image was analyzed and the distance versus frame number and time respectively (record speed was equal to 1 fps) was determined. The different starting points are given by setting $t_0 = 0$ s by the onset of the solidification of the first grain within the sample. For a freely growing dendrite with progressing time and therefore increasing undercooling according to the Lipton-Glicksman-Kurz model²⁵⁾ an increase in dendrite tip velocities is expected. With progressing time solutal-field interaction between growing dendrites of neighboring grains becomes more and more important. This leads to dendrite tip velocities running through a maximum and decreasing at later solidification times. This has been observed in in-situ experiments reported by Bogno et al.²⁶⁾. We observe a similar behavior (cf. **Fig. 8**). It is shown that fluid-flow leads in our case to up to a factor three increased dendrite tip velocity at the maximum growth velocity compared to a randomly chosen dendrite growing under more homogeneous conditions and suppressed convective fluid flow (X-RISE vertically aligned; quasi 2D sample perpendicular to the gravitational force).

The vertically rotatable X-RISE facility enables to systematically investigate the influence of fluid flow on dendritic microstructure evolution in the laboratory and to validate growth theories and phase field models under different convective conditions.

2.2.5 Linear Shear Cell - LSC

A compact-sized shear cell for in-situ interdiffusion measurements in liquid alloys shown in **Fig. 9** was used to measure the impact of gravity driven fluid flow during a parabolic flight campaign. Within outer dimensions of $40 \times 40 \times 20$ mm, the shear cell contains seven samples resulting in six diffusion couples in

long capillaries which remain spatially separated during melting, homogenization and optional μg -injection. The diffusion is then initiated (cf. bottom left of Fig. 9) by moving one part of the shear cell. Through diffusion the initial concentration difference is equalized (cf. bottom right of Fig. 9). A detailed description of the shear-cell furnace and its operation can be found in references^{5,27}.

3. Diffusion Experiment During Parabolic Flight

In the parabolic flight experiment shown here the alignment of the long-axis of the samples is initially perpendicular to the gravitational force (beam alignment vertical) in order to use the convection for homogenization of the samples after melting. The X-ray experiment unit is then tilted by 90° with the seven samples parallel to gravitational force (beam alignment horizontal) before the diffusion processes is initiated by shearing the bottom half of the LSC resulting in six diffusion couples. The diffusion process was started during a 1g-phase ahead a μg parabola. The diffusion couples are aligned such that under 1g conditions for each capillary the denser material is at the bottom and the less dense material is at the top of the liquid column. The same applies for the hyper-gravity phase. A first data set was gained during this phase. Furthermore diffusion data were determined during the hyper-g phase (2g-phase) were the aircraft pull up into a steep climb before the μg -phase (flight trajectory is parabola like). The

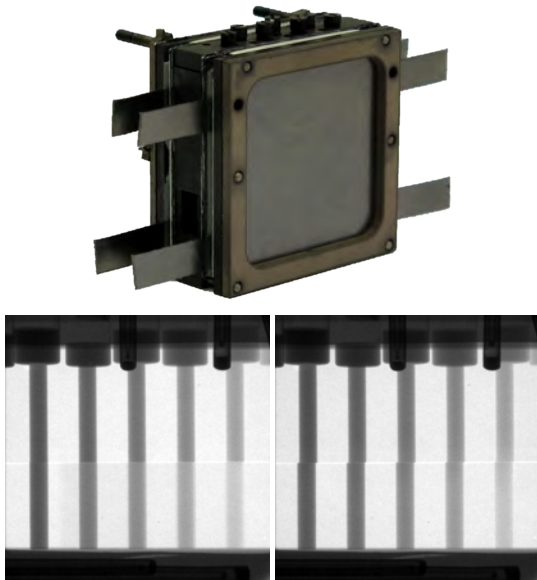


Fig. 9 Photograph of the linear shear cell. The X-ray image of the LSC showing the configuration of the LSC with its different $\text{Al}_{1-x}\text{Cu}_x$ ($x=0..22.5$ at%) alloys. The left picture was taken immediately after shearing, whereas the right radiograph shows the diffused Al-Cu samples. Shearing means a sliding operation of the bottom part of the sample containing crucible to the left.

X-ray images taken under reduced gravity conditions were analyzed as a third set of data points. Finally data collected during the second hyper-gravity phase were evaluated when the drop of the plane is stopped by a pull-out maneuver.

4. Results of the Interdiffusion Experiment on $\text{Al}_{1-x}\text{Cu}_x$ ($x=0, \dots, 22.5$ at%)

The diffusion coefficients of five different Al-Cu diffusion couples processed during the parabolic flight could be evaluated. The samples were heated to a temperature of 973 K. The liquid alloys experienced a change of the gravitational field after shearing from 1g to 2g to μg and back to 2g. To gain concentration profiles from the X-ray images, the measured gray values at each position have to be normalized using procedures described in Ref. 28). The obtained diffusion profiles for Al-Cu are fitted with the appropriate solution of Fick's 2^{nd} law of diffusion (cf. Fig. 10). The resulting fit parameter $4Dt$ with the diffusion coefficient D and the time t exhibits a clear change in slope during the μg -phase, as shown in Fig. 11. The corresponding diffusion coefficients for all five

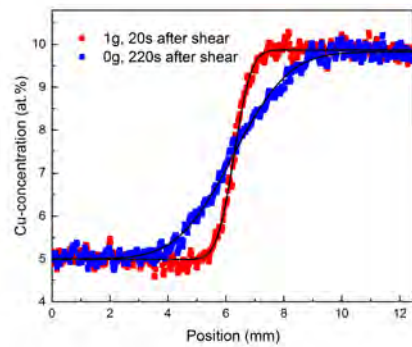


Fig. 10 Diffusion profiles of Al-5%Cu versus Al-10%Cu extracted from two different radiographs taken 20 seconds after shearing (1g-phase) and 220 seconds after shearing (reduced gravity-phase). Solid lines are fits with an error function.

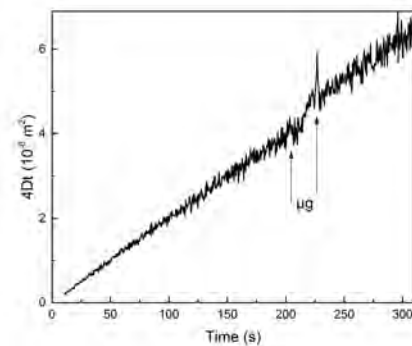


Fig. 11 Parameter $4Dt$ with diffusion coefficient D and time t as a function of time.

diffusion couples for the different gravity-phases are derived from the corresponding slopes and plotted in **Fig. 12**. For the measurements a microfocus X-ray source with 80 kV and up to 10 W in combination with the RadEye detector was used. The detector frame rate was set to 1 Hz, which gives good contrast-properties. Sample-source-detector distances were set such that a total resolution of 21 μm corresponding to sample plane was achieved.

Interestingly the diffusivity under μg conditions is higher than the diffusion values determined under normal and hyper-g phases. Fluid flow, which can be caused by buoyancy, leads to a higher apparent diffusion coefficient. Under 1g and hyper-g conditions a stable density layering of the different alloy concentrations damped convection at least to a certain extent^{20,29,30}. Surprisingly the μg data yield higher values for the diffusion coefficient. We believe that this is caused by the so-called g-gitter, where a negative g-acceleration caused by the flight maneuver destabilizes the density layering leading to strong fluid flow effects inside the capillaries. This clearly shows that benchmark data has to be measured on longer duration platforms with better μg quality like sounding rockets, reentry capsules or space stations.

5. Conclusion

A new multifunctional facility for parabolic flight and laboratory research activities by the means of in-situ and real time X-ray radiography is introduced including all existing experiment inserts which were developed during the last 2 years. Microgravity experiments on granular matter as well as on liquid metallic alloy diffusion are presented. Moreover the rotatable X-RISE facility could be used to investigate solidification experiments via X-ray radiography on quasi 2-dimensional metallic alloys under terrestrial conditions where fluid flow could geometrically be minimized such that almost undisturbed equiaxed dendritic growth could be studied.

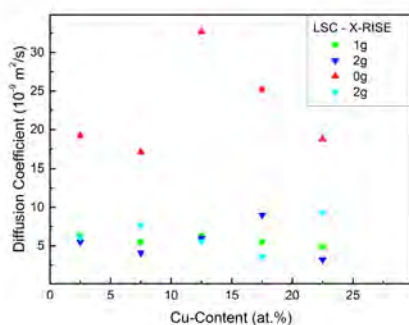


Fig. 12 Data obtained during the parabolic flight campaign. First transition from 1g-phase to hyper g-phase (2g), to μg -phase, and back to hyper g-phase evaluated after shear of the cell at a temperature of 973 K.

Acknowledgments

We acknowledge P. Born for fruitful discussions and proof-reading the manuscript. We thank P. Barmesen and S. Grüter for the original development and construction of the isothermal and high temperature gradient furnace respectively and workshop team of the Institute, namely, K. Afanasev, M. Nell, H. Esser, and R. Henrichs for the excellent support in getting X-RISE parts ready in time. We thank NOVESPACE for support during the campaigns and the district government of Cologne in particular D. Höwekemeier for his advices as well as the French Nuclear Safety Authority for their excellent support getting the acceptance for the operation of X-RISE not only in the laboratory at DLR in Cologne but also aboard the parabolic flight.

References

- 1) E. Lombi and J. Susini: *Plant and Soil*, **320** (2009) 1.
- 2) R. Meuli, Y. Hwu, J. H. Je and G. Margaritondo: *European Radiology*, **14** (2004) 1550.
- 3) T. Schenk, H. Nguyen-Thi, J. Gastaldi, G. Reinhart, V. Cristiglio, N. Mangelinck-Noël, H. Klein, J. Härtwig, B. Grushko and B. Billia: *J. of Crystal Growth*, **275** (2005) 201.
- 4) F. Beckmann, R. Grupp, A. Haibel, M. Huppmann, M. Nöthe, A. Pyzalla, W. Reimers, A. Schreyer and R. Zettler: *Advanced Engineering Materials*, **9** (2007) 939.
- 5) C. Neumann, E. Sondermann, F. Kargl and A. Meyer: *J. of Physics, Conference Series*, **327** (2011) 012052.
- 6) R. H. Mathiesen, L. Arnberg, F. Mo, T. Weitkamp and A. Snigirev: *Physical Review Letters*, **83** (1999) 5062.
- 7) H. Nguyen-Thi, H. Jamgotchian, J. Gastaldi, J. Härtwig, T. Schenk, H. Klein, B. Billia, J. Baruchel and Y. Dabo: *J. of Physics D, Applied Physics*, **36** (2003) A83.
- 8) H. Yasuda, I. Ohnaka, K. Kawasaki, A. Sugiyama, T. Ohmichi, J. Iwane and K. Umetani: *J. of Crystal Growth*, **262** (2004) 645.
- 9) R. H. Mathiesen, L. Arnberg, P. Bleuet and A. Somogyi: *Metallurgical and Materials Transactions, A*, **37** (2006) 2515.
- 10) R. H. Mathiesen, L. Arnberg, H. Nguyen-Thi and B. Billia: *JOM*, **64** (2012) 76.
- 11) A. Bogno, H. Nguyen-Thi, A. Buffet, G. Reinhart, B. Billia, N. Mangelinck-Noël, N. Bergeon, J. Baruchel and T. Schenk: *Acta Materialia*, **59** (2011) 4356.
- 12) G. Reinhart, C.-A. Gandin, N. Mangelinck-Noël, H. Nguyen-Thi, J.-E. Spinelli, J. Baruchel and B. Billia: *Acta Materialia*, **61** (2013) 4765.
- 13) H. Nguyen-Thi, G. Reinhart, G. Salloum Abou Jaoude, R. H. Mathiesen, G. Zimmermann, Y. Houltz, D. Voss, A. Verga, D. J. Browne and A. G. Murphy: *J. of Crystal Growth*, **374** (2013) 23.
- 14) B. M. Patterson, K. C. Henderson, P. J. Gibbs, S. D. Imhoff and A. J. Clarke: *Materials Characterization*, **95** (2014) 18.
- 15) S. Reisinger, A. Ennen, T. Wörlein, M. Schmitt and V. Volland: *4th International Symposium on NDT in Aerospace*, **3** (2012).
- 16) M. Becker, C. Dreißigacker, S. Klein and F. Kargl: *Review of Scientific Instruments*, **86** (2015) 063904.
- 17) F. Kargl, M. Balter, C. Stenzel, T. Gruhl, N. Daneke and A. Meyer: *J. of Physics, Conference Series*, **327** (2011) 012011.

- 18) P. Yu, S. Frank-Richter, A. Börngen and M. Sperl: *Granular Matter*, **16** (2014) 165.
- 19) G. Reinhart, N. Mangelinck-Noël, H. Nguyen-Thi, T. Schenk, J. Gastaldi, B. Billia, P. Pino, J. Härtwig and J. Baruchel: *Materials Science and Engineering, A*, **413** (2005) 384.
- 20) F. Kargl, E. Sondermann, H. Weis and A. Meyer: *High Temp. High Press.*, **42** (2013) 3.
- 21) R. Son, J. A. Perez and G. A. Voth: *Physical Review* **E78** (2008) 041302.
- 22) D. M. Herlach: *Metals*, **4** (2014) 196.
- 23) W. J. Boettinger, J. A. Warren, C. Beckermann and A. Karma: *Annual Review of Materials Research*, **32** (2002) 163.
- 24) L. Yuan and P. D. Lee: *Modelling and Simulation in Materials Science and Engineering*, **18** (2010) 055008.
- 25) J. Lipton, M. E. Glicksman and W. Kurz: *Metallurgical Transactions* **A18** (1987) 341.
- 26) A. Bogno, H. Nguyen-Thi, B. Billia, N. Bergeon, N. Mangelinck-Noël, E. Boller, T. Schenk and J. Baruchel: *Transactions of the Indian Institute of Metals*, **62** (2009) 427.
- 27) E. Sondermann, C. Neumann, F. Kargl and A. Meyer: *High Temp. High Press.*, **42** (2013).
- 28) A. Griesche, B. Zhang, E. Solórzano and F. Garcia-Moreno: *Review of Scientific Instruments*, **81** (2010) 056104.
- 29) S. Suzuki, K.-H. Kraatz and G. Froberg: *Microgravity Science and Technology*, **16** (2005) 120.
- 30) A. Meyer and F. Kargl: *Int. J. Microgravity Sci. Appl.*, **1** (2013) 30.

Appendix

Figure 13 illustrates the main components of X-RISE and their logical conjunction as for instance pumping units for vacuum creation or the cooling water circuit.

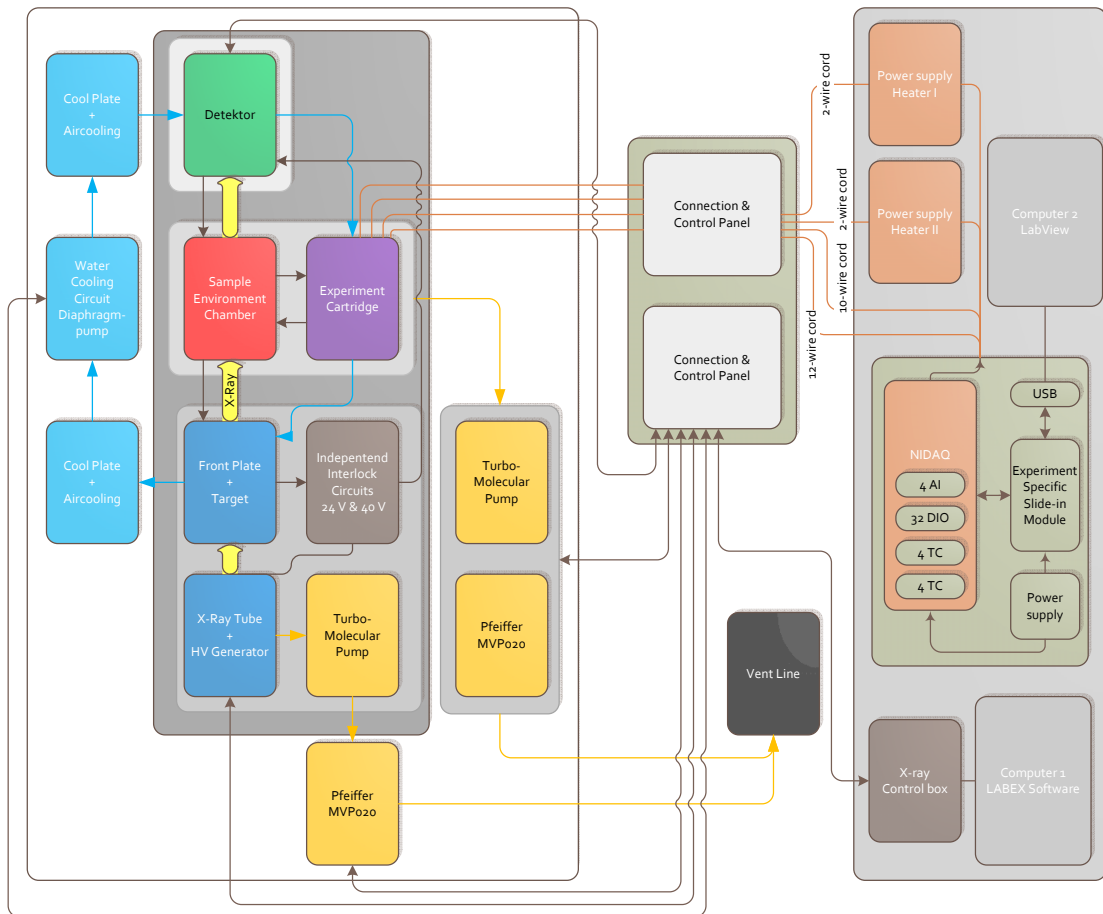


Fig. 13 The scheme shows the main components of X-RISE. On the left, the experiment rack with the rotatable X-ray unit consisting of the tube, sample chamber, and detector is visualized. On the right, the control rack with the computers and controllers is drafted.